APL Photonics

RESEARCH ARTICLE | APRIL 15 2025

Dual fiber probe with 3D-printed micro-lens for Brillouin microscopy

Special Collection: Brillouin Scattering and Optomechanics

Joshua Trapp ; Hadi Mahmodi ; Marco Wende ; Luke McAlary ; Lezanne Ooi ; Jiawen Li ; Robert A. McLaughlin ; Alois Herkommer ; Andrea Toulouse ; Irina Kabakova

APL Photonics 10, 040803 (2025)
https://doi.org/10.1063/5.0238060

Dual fiber probe with 3D-printed micro-lens for Brillouin microscopy

Cite as: APL Photon. 10, 040803 (2025); doi: 10.1063/5.0238060
Submitted: 9 September 2024 • Accepted: 26 March 2025 •
Published Online: 15 April 2025

Joshua Trapp,[1,2,a] Hadi Mahmodi,[3,b] Marco Wende,[1,4,c] Luke McAlary,[5,d] Lezanne Ooi,[5,e] Jiawen Li,[6,7,f] Robert A. McLaughlin,[7,8,g] Alois Herkommer,[1,4,h] Andrea Toulouse,[1,4,i] and Irina Kabakova[3,i]

AFFILIATIONS

[1] Institute of Applied Optics (ITO), University of Stuttgart, 70569 Stuttgart, Germany
[2] Graduate School of Excellence Advanced Manufacturing Engineering GSaME, Allmandring 35, 70569 Stuttgart, Germany
[3] School of Mathematical and Physical Sciences, University of Technology Sydney, Harris Street, Building 4, 2007 Sydney, Australia
[4] Research Center SCoPE, University of Stuttgart, Pfaffenwaldring 57, 70569 Stuttgart, Germany
[5] Molecular Horizons and School of Science, University of Wollongong, Northfields Ave., Wollongong, New South Wales 2522, Australia
[6] School of Electrical and Mechanical Engineering, The University of Adelaide, 5005 Adelaide, Australia
[7] Institute of Photonics and Advanced Sensing, The University of Adelaide, 5005 Adelaide, Australia
[8] Faculty of Health and Medical Sciences, The University of Adelaide, 5005 Adelaide, Australia

Note: This paper is part of the APL Photonics Special Topic on Brillouin Scattering and Optomechanics.

[a] joshua.trapp@ito.uni-stuttgart.de
[b] Hadi.MahmodiSheikhSarmast@uts.edu.au
[c] wende@ito.uni-stuttgart.de
[d] lmcalary@uow edu.au
[e] lezanne@uow.edu.au
[f] jiawen.li01@adelaide.edu.au
[g] robert.mclaughlin@adelaide.edu.au
[h] herkommer@ito.uni-stuttgart.de
[i] **Authors to whom correspondence should be addressed:** toulouse@ito.uni-stuttgart.de. **Telephone:** +49 711 685 66648 and Irina.Kabakova@uts.edu.au. **Telephone**: +61 2 9514 4830

ABSTRACT

Brillouin spectroscopy is a powerful technique for non-invasive micromechanical analysis of biological materials such as tissues and cells. Conventional bulk-optical Brillouin spectroscopy systems, however, face challenges in translation to endoscopic applications due to strong parasitic background signals using single optical fibers. To overcome this issue, dual fiber approaches have been proposed, but they suffer from poor overlap of excitation and collection beam paths. In this work, we present a dual fiber-integrated probe with a tip diameter below 300 μm. Using tailored freeform 3D-printed micro-optics, we achieve a precise overlap of the foci to map mechanical properties with a resolution below 10 μm in lateral and 45 μm in axial direction. We detail the probe's design, fabrication, and optical simulations and present experimental results demonstrating high-resolution Brillouin measurements from polymer and protein solution samples. Our findings indicate that this dual fiber probe could significantly advance fiber-integrated Brillouin spectroscopy, with promising applications in materials science and biomedical diagnostics.

INTRODUCTION

Brillouin spectroscopy has emerged as a powerful technique for non-invasive analysis of mechanical properties in various materials, including biological tissues. Its ability to measure acoustic phonons provides valuable insights into the microscopic viscoelastic properties of samples, which is particularly beneficial in biomedical applications.[1,2] Prominent applications for the mechanical analysis of tissues include diagnosis of osteoarthritis, delineation and analysis of cancer, and atherosclerosis,[3–7] the latter two being among the leading causes of death worldwide.[8,9]

Conventional Brillouin spectroscopy systems are unsuitable for endoscopy applications (such as imaging inside joints, airways, blood vessels, and the gastrointestinal tract) due to their bulkiness, which prevents access to confined spaces. Fiber-based Brillouin systems are desirable for endoscopic applications as these can be small and flexible [Fig. 1(a)]. However, fiber-integrated Brillouin applications are hindered by a parasitic background signal originating from the optical fiber core. The parasitic signal exhibits significantly higher intensity compared to the desired signal originating from the focal point within the sample. This is because the fiber core has a small effective mode area in which light is highly concentrated. Therefore, even a single meter of a standard optical fiber will generate a Brillouin signal that would be orders of magnitude higher than any scattering in the sample. Such a high relative intensity parasitic signal can make it difficult to extract the signal of interest, highlighting the need to minimize the parasitic background.[10,11]

This problem can be addressed by using hollow-core fibers, thus preventing Brillouin light scattering in the fiber core. However, hollow core fibers are fragile and not compatible with standard commercial components such as circulators and couplers, which hinders the integration into established Brillouin spectroscopy setups. On the other hand, single-mode step-index fibers with standardized connectors (e.g., FC/APC) enable practical integration and facilitate the use of common, low-cost components.[11,12]

Prior studies have demonstrated that a dual step-index fiber approach can be used to decouple the background signal from the sample signal.[10] In this approach, the laser light is launched from one fiber and collected by a second fiber. Brillouin scattering occurs only in the backward direction. Therefore, the parasitic background is only contained in the launch fiber and does not leak into the collection fiber. Consequently, the parasitic background is not observed in measurements through the collection fiber. However, conventional optical elements such as gradient-index (GRIN) lenses are ill-suited for use in a dual fiber setup. The focal spots of both fibers should meet in the same spot in the sample. This is required to collect the signal from where it is created. A rotationally symmetric element (e.g., a GRIN lens) cannot focus two parallel fields into one point. To achieve this, a free form off-axis optical element is required.[10] In Fig. 1, we present wave-optics simulations highlighting three approaches. To summarize the content of Fig. 1: Focusing the input beam of a single-mode fiber with a generic aspheric lens or GRIN lens [Fig. 1(b)] is favorable from an optics manufacturing perspective but suffers from a parasitic background Brillouin signal generated within the fiber core in the backward traveling direction.[10] A dual bare fiber approach [Fig. 1(c)] eliminates the parasitic signal from the input fiber. However, without suitable optics, the fields of the two fibers have negligible overlap [Fig. 1(c)], resulting in a poor spatial resolution and weak signal strength. Figure 1(d) presents the approach proposed in this work, combining the high spatial confinement of the Fig. 1(b) approach with the dual fiber solution of Fig. 1(c). Two-photon lithography (TPL) has proven well suited for the manufacture of such miniaturized, high performance optical elements. The quality of these miniaturized TPL optics has been demonstrated in fiber-optic endoscopic imaging systems to enable minimally invasive diagnostics;[13–16] however, not in Brillouin spectroscopy.

In this paper, for the first time, we present a dual fiber Brillouin probe that utilizes a 3D-printed freeform lens. We outline the ray optical design and additional wave-optical characterizations that have guided the design process. Our experimental results demonstrate the probe's ability to acquire high-resolution Brillouin signals from various 3D-printed structures and a biological sample of a phase-separated DDX4 protein.[17] The acquired Brillouin signal is free from the parasitic background that was observed in previous studies.[10] Due to the utilization of conventional single-mode fibers, the probe is easy to integrate into an existing Brillouin spectroscopy setup.

The probe's compact size and over eight-times enhanced signal intensity compared to a bare dual fiber setup can offer a promising path toward *in vivo* and *in situ* measurements, including micromechanical tissue endoscopy. Compared to previous dual fiber GRIN lens approaches, which were only collecting efficiently enough to retrieve single point spectra from clear liquids, the new probe design enables the sampling of entire 2D areas of a specimen.[10] Our findings highlight the potential of this dual fiber probe to advance the field of fiber-integrated Brillouin imaging, paving the way for new applications in biomedical diagnostics and materials science.

MATERIAL AND METHODS

Optical design and simulation

For the design of the probe, we utilize the ray optics simulation software Zemax OpticStudio (Ansys Inc., USA). The derived design is illustrated in Fig. 2. Two telecentric fields with an NA of 0.12 (NA of the optical fiber) and a 125 μm spacing in the y-direction were considered. We optimized for diffraction limited focusing of both fields into a single spot.

For wave-optical simulations, we used a custom implementation of the wave propagation method.[18] A sampling step size of dy = dz = 0.08 μm, n = 1.5081 for the lens material,[20] and n = 1.331 for the environment (water).[21] The light emitted by the fibers was modeled as electric fields (wavelength = 660 nm) with telecentric propagation direction and a Gaussian envelope curve that matches the mode field diameter (d = 4.45 μm) of the fiber core (see Ref. 19 for more details). For comparison with the measurements, we computed the intensity from the electric fields calculated in the WPM simulations.[22]

Micro-lens fabrication

From the ray optical design file, we imported the mechanical data of the optimized micro-lens into Computer-Aided Design (CAD) software (SolidWorks, Dassault Systèmes, France) and added

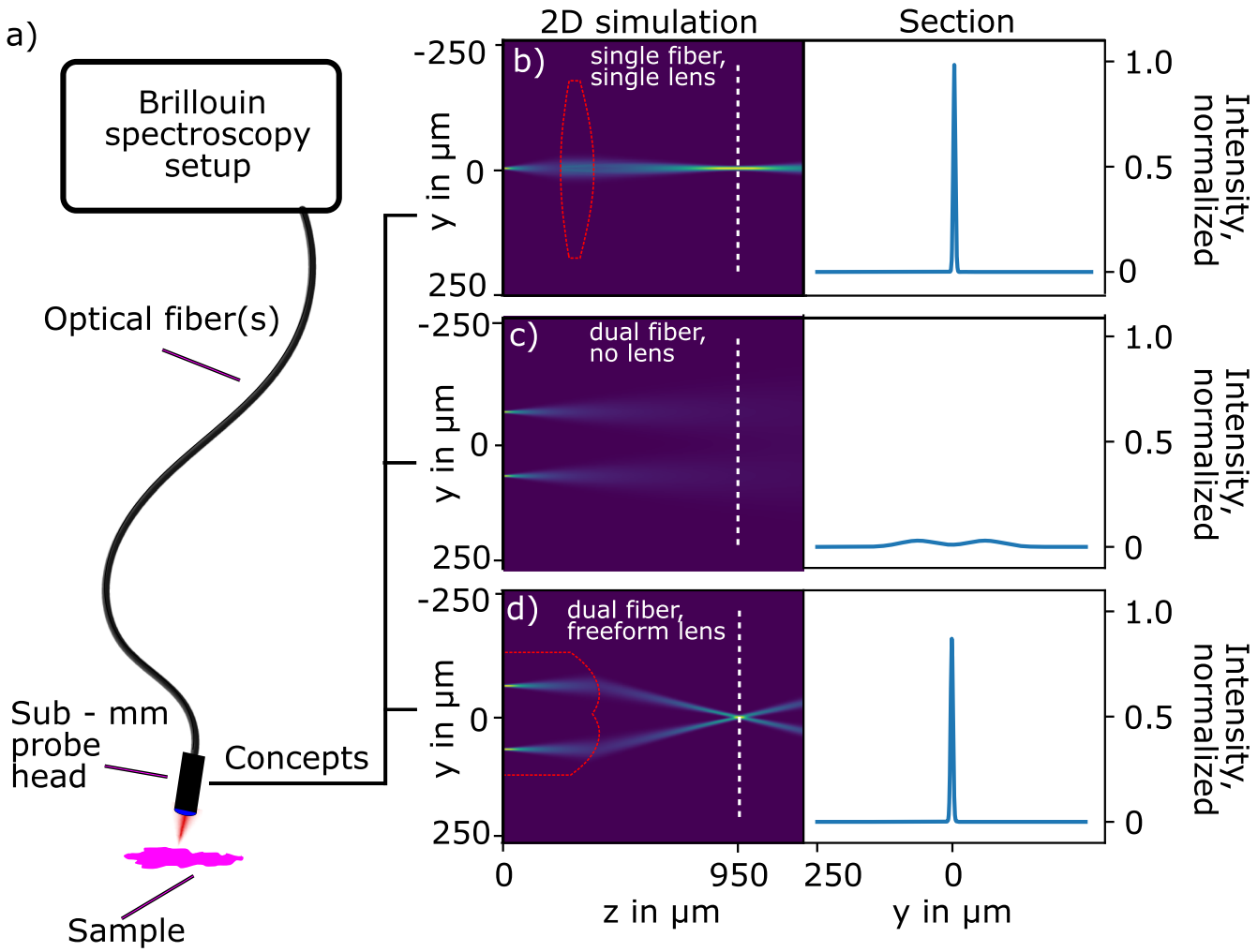

FIG. 1. Concepts for fiber-integrated Brillouin spectroscopy. (a) Simplified setup of fiber-integrated implementations. [(b)–(d)] Wave-optical simulation of different potential fiber/lens arrangements: (b) single fiber with a generic rotationally symmetric aspheric lens, (c) two adjacent bare optical fibers without lens elements, and (d) two adjacent optical fibers with off-axis conic freeform lenses to intersect the two fiber mode fields in their focal spots.

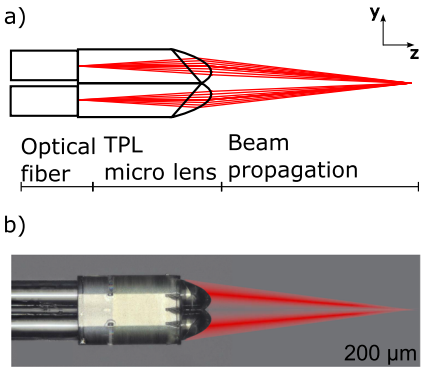

FIG. 2. Optical design and fabricated Brillouin fiber probe. (a) Ray optical conic off-axis freeform design of the dual fiber probe. (b) Two-photon lithography fabricated a freeform lens, mounted on and fixing two optical single-mode fibers. The mode propagation is indicated for visualization.

mechanical supports. The micro-lens was fabricated using TPL with a Photonic Professional GT2 (Nanoscribe GmbH, Germany). The material of the probe is IP-S.[23] The writing process employed a 25x, 0.8 NA immersion objective (Plan-Apochromat 25×/0.8, Carl Zeiss Microscopy, Germany). We chose a laser power of 40 mW and a slicing and hatching of 0.1 μm for the optical surface of the probe. For the bulk material of the probe, we reduced the slicing and hatching to 0.3 µm to increase the process speed. The dual fiber micro-lens was printed onto an Indium Tin Oxide (ITO) coated glass substrate. After TPL fabrication, the micro-lens was attached to two single-mode fibers (P3–630Y, Thorlabs Inc., USA). The process of connecting micro-optics to fibers as a post-process has been described in earlier publications.[24] The two optical fibers terminate in FC/APC connectors.

Post-writing, the fabricated micro-lens was developed to remove unpolymerized resin through a three-step process: 15 min immersion in propylene glycol methyl ether acetate (PGMEA), followed by 5 min in 2-propanol (PGMEA and

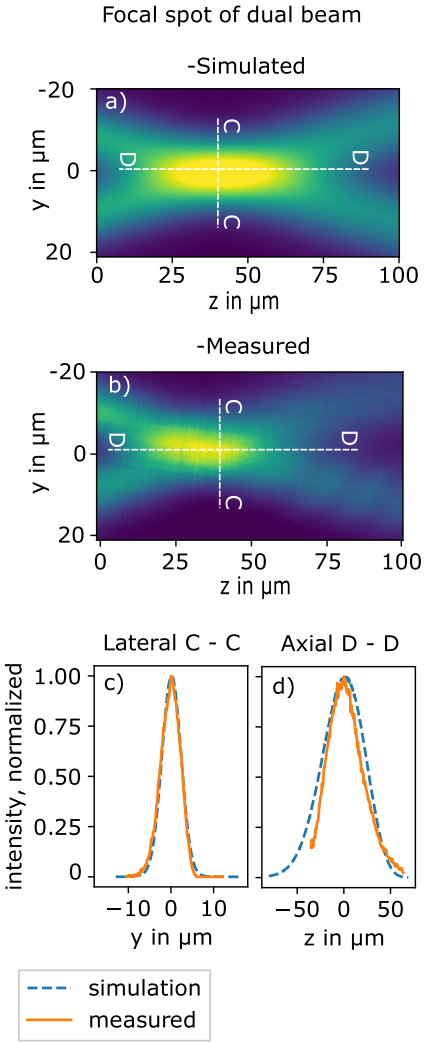

FIG. 3. Point spread function (PSF) measurement and simulation of the fiber probe. (a) y-z plane of the probe—simulated in wave propagation method. (b) y-z plane of the probe—measured. (c) Section of the lateral intensity profile of the PSF, full width half maximum of 5.3 μm (both measurement and simulation). (d) Section along the fiber axis, FWHM of 53 μm for the simulation and 43 μm for the measurement. The lateral and axial sections in [(a) and (b)] are indicated by dashed lines and the corresponding letters.

2-propanol provided by Merck KGaA, Germany), and subsequent air-drying at room temperature. The resulting fiber probe is shown in Fig. 2(b).

PSF measurements

We used a microscope objective with an NA of 1.2 and a magnification of 40× (Plan-Apochromat 40×/1.2, Carl Zeiss Microscopy, Germany) to image the focal spot of the probe in water on a CCD sensor. The microscope objective was mounted on a piezo-driven z-axis stage (P721k137, Physik Instrumente (PI) GmbH, Germany), allowing precise movement along the optical axis. The scanning was performed with a step size of 0.5 μm over a total scan length of 100 μm. At each scan step, an image was acquired, resulting in a 3D image stack of the probe PSF[25] (section through image stack in Fig. 3).

Brillouin scattering measurement

The schematic of the setup for characterizing the dual fiber Brillouin probe is depicted in Fig. 4. The sample illumination is provided by a continuous-wave laser (660 nm, 120 mW, Torus, Laser Quantum, by Novanta Photonics, USA), coupled into the input channel of the dual fiber Brillouin probe via a fiber coupler. The output from the second channel of the dual fiber Brillouin probe is collimated by a 75 mm lens and then focused by a 300 mm lens through the aperture of a 6-pass scanning tandem Fabry–Pérot interferometer (TFP1, Table Stable Ltd., Switzerland).[26]

The spectral resolution of our Fabry–Pérot interferometer is defined by the 3 mm mirror separation, resulting in 512 spectral points in each spectrum with a spectral resolution of ~276 MHz. The system's spectral extinction ratio between the Brillouin signal and background noise for this spectrometer surpasses 10.[10,23]

For accurate data acquisition, the setup utilized Ghost software (provided by The Table Stable Ltd., Switzerland) for single-point measurements. The raw spectra of Brillouin scattered light were analyzed using the Lorentzian model, where the peak positions are used to determine the Brillouin frequency shift.

The resin spectra (Fig. 5), collected by a bulk optical Brillouin system, were acquired with an acquisition time of 20 seconds.

A more detailed description of the utilized Brillouin spectroscopy system (excluding the fiber probe) has been published previously.[27,28]

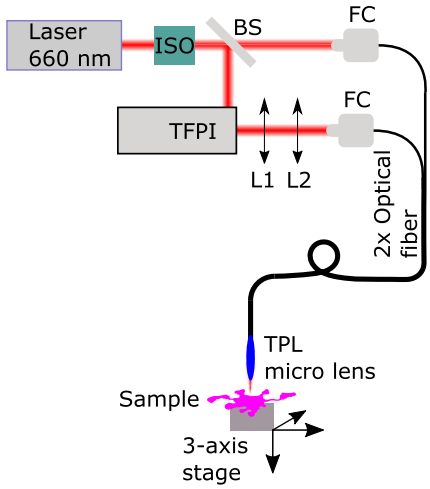

FIG. 4. Simplified illustration of Brillouin scatter setup. A 660 nm laser is divided by a beam splitter. The first beam is coupled into the fiber probe through a FC/PC connector. The second beam is directed into a tunable Fabry–Pérot interferometer (TFPI). The light that is coupled into the fiber probe is focused by a freeform micro-lens element onto a sample. The fiber probe is mounted stationary, while the sample is positioned by a three-axis stage. Scattered light is collected from the sample and coupled back into the fiber probe. The scattered light that is transmitted through the second fiber of the probe is coupled into the TFPI.

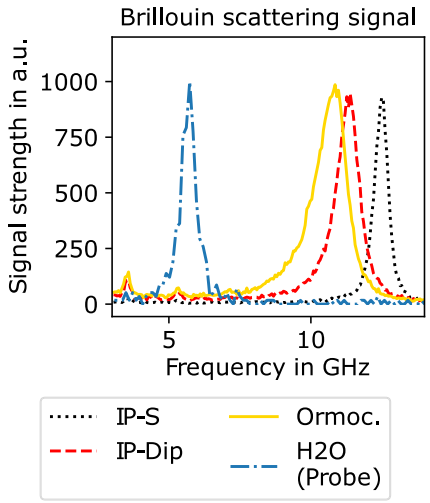

FIG. 5. Brillouin scattering signals of different photoresins in their polymerized state and water. A bulk-optical confocal Brillouin scattering microscope was used to acquire the signals of the photoresins. The signal of water is acquired with the presented dual fiber probe. The water signal collected by the probe has no visible signal from IP-S (material of the probe's micro-lens).

Linear and 2D scans with Brillouin probe

Linear and 2D scans were executed by manipulating the position of the sample on a 3D microscopy stage (SmarAct, Germany). The microscopy stage manipulated the sample in x, y, and z while the fiber probe was fixed on an optical post. In-house software facilitated two-dimensional (2D) scans within the sample plane with an acquisition time of 120 seconds per point.

Samples

The first 2D sample, displayed in Fig. 7(a), is a 3D-printed sample featuring the letters "UTS." This sample was produced via stereolithography using Clear Resin V4 (Formlabs, United States). The scanned area of the sample measures 5.25 × 7.65 mm, with a scanning pitch of 0.15 mm.

In addition, a chirped line target was fabricated for lateral and axial scanning tests with the fiber probe. The target consists of three sets of lines. Each set has three lines with a pitch of 40, 20, and 10 μm for the first, second, and third sets, respectively [Fig. 6(a)]. The target was designed within CAD software (SolidWorks) and exported as an STL file. In the TPL fabrication, the utilized microscope objective had an NA of 1.4 with a magnification of 40× (Plan-Apochromat 40×/1.4, Carl Zeiss Microscopy, Germany). Chirped line targets were fabricated using IP-DIP 2 (Nanoscribe GmbH, Germany).

In addition, we acquired a 2D Brillouin map of a sample containing phase-separated DDX4 protein droplets immersed in water [Fig. 7(e)]. The sample was scanned with a stage pitch of 2 μm and with an acquisition time of one minute per point. DDX4 protein was expressed in bacteria and purified. DDX4 stored at a concentration of 300 μM in a buffer of 20 mM Tris and 500 mM NaCl (pH 8.0) with 2 mM β-mercaptoethanol was phase separated by dilution in 20 mM MES (pH 6.0) at a 1:3 ratio of DDX4 buffer to MES buffer.[17]

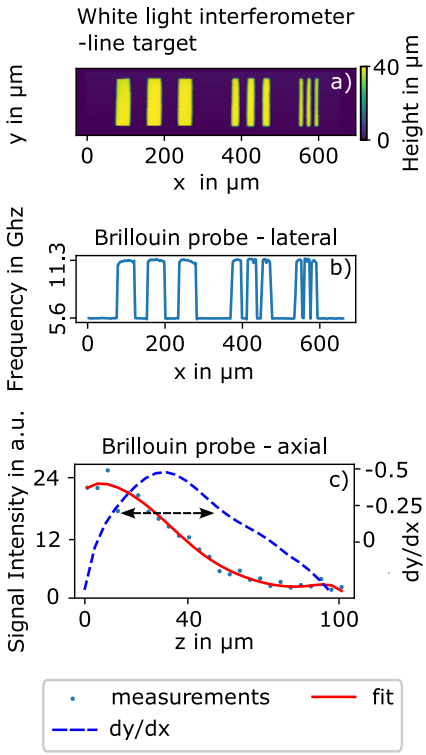

FIG. 6. Lateral and axial resolution of the fiber-integrated Brillouin probe. The displayed lines have a pitch and width of 40, 20, and 10 μm. (a) Spatial arrangement of a chirped line target, measured by white light interferometry, (b) Brillouin line scan across the chirped target, and (c) axial scan across an interface of water and glass. The black dashed line indicates the full width half maximum of the negative part of dy/dx.

Spectroscopy data processing

The raw spectra comprising Brillouin peaks (both Stokes and anti-Stokes) were analyzed using the damped harmonic oscillator model to determine the Brillouin frequency shift. To reduce noise in measurements of protein liquid–liquid phase separation, we applied a non-linear 3 × 3 smoothing kernel using MATLAB's "medfilt2" function [Figs. 7(c) and 7(d)]. This approach is justified as the measurement step was 3 μm, which is below the probe's resolution limit, hence presenting us with oversampled data.

RESULTS

Optical design

For the excitation beam path, the rays at the 660 nm wavelength are expanded from the fiber core through a length of 390 μm bulk material and focused by a conic off-axis freeform lens [Fig. 2(a)] into an aqueous environment (n = 1.33). The optical surface is non-rotationally symmetric to achieve an off-axis focal spot, placed between the excitation and collection fibers (Fig. 2).

This design results in a numerical aperture (NA) of 0.06 and a focal length of 600 μm, targeting a lateral deviation of 62.5 μm from the optical axis in the y-direction. The ray optical design has a diffraction limited performance with an Airy radius of 6.4 μm and

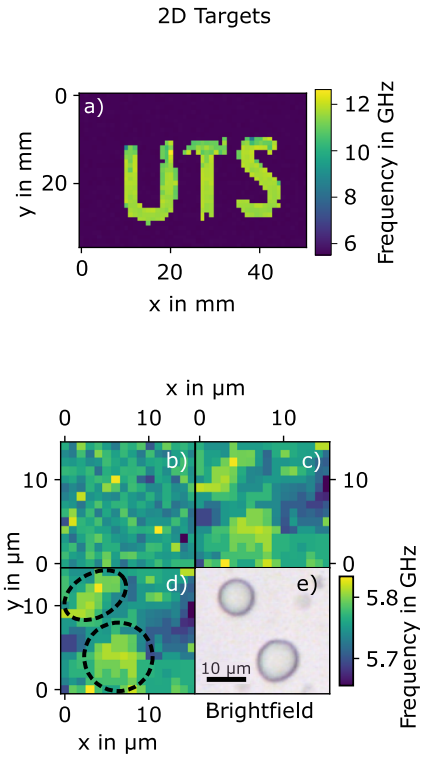

FIG. 7. Brillouin imaging by means of the fiber probe. (a) 2D scan of a 3D-printed sample with the letters "UTS." (b)–(d) 2D scan of protein droplets in solution: (b) raw data, (c) smoothed data with a 3 × 3 non-linear kernel, (d) smoothed data with droplets highlighted, and (e) bright-field microscope image of protein droplets in the solution.

a FWHM of 5.2 and 5.6 μm in the x and y directions. The lateral offset was chosen according to the radius of the optical fiber. For the collection fiber, this off-axis element is mirrored at the xz-plane, creating an overlap of excitation and collection fiber spots at the focal position. The dimensions of this probe are 160 × 285 μm^2 (x and z directions).

Characterization of the probe design

To validate the ray optical design, we conducted an additional wave-optical simulation using the wave propagation method (WPM).[18,19] The predicted focus in the overlap-region between the two beams [Figs. 3(a) and 3(b)] confirms the validity of the ray optical design. Experimentally, we characterized the point spread function (PSF) of our fabricated probe using a 660 nm laser coupled into both fibers simultaneously. An axial cut through the y-z plane of the acquired 3D PSF is shown in Fig. 3(b). The full width at half maximum (FWHM) spot size in the lateral direction shows good agreement with the wave-optical simulation (both 5.3 μm). Furthermore, the lateral spot extension aligns well with the ray optical model, indicating performance close to the diffraction limit. This suggests that the micro-lens does not suffer from significant optical aberrations. However, the axial FWHM appears shorter in the measurements (43 μm) compared to the wave-optical simulation results (53 μm). This discrepancy can be attributed to slight deviations in the production outcome compared to the ideal simulation scenario. In Fig. 3(d), it can be observed that the intensity profile of the measured PSF deviates from an ideal Gaussian beam, which leads to an altered FWHM of the measured PSF. Furthermore, manufacturing tolerances in the alignment of the fiber and micro-lens can contribute to this issue. In particular, the spacing between the fibers and any gap between the fiber and the micro-lens are critical factors. A separation between the fibers causes the two beam paths to intersect at a steeper angle, thereby reducing the overlap of the focal spots in the axial direction.

In addition, a gap between the fiber and the micro-lens increases the numerical aperture (NA) of the optical system (the beam can expand more before it is focused). Since the axial spot size is proportional to the square of the NA, this could lead to a reduction in the axial spot size.

Brillouin signal acquisition

To verify the effectiveness of the dual fiber probe device with a micro-lens, we measure the strength of the Brillouin scattering signal collected by our device in distilled water. For reference, we compare it with a lensless dual fiber arrangement [Fig. 1(b)]. We detect an 8.14 times stronger signal (mean values) collected by the device with our freeform micro-lens compared to the probe without any lens (Fig. 8).

Furthermore, to show the clear distinction between the Brillouin spectra of the TPL photoresist and a material such as water, we recorded the Brillouin spectra of three TPL photo resins: IP-S, IP-DIP 2, and OrmoComp. These correspond to the materials used to fabricate the micro-lens (IP-S), the material used to fabricate the line target in section "Spatial and Frequency Resolution" (IP-DIP 2), and OrmoComp, a material commonly used in TPL processes due to its favorable properties like high transparency in the visible wavelength.[20] The Brillouin spectra for these resins (Fig. 5) were collected using a bulk-optical microscopy setup.

Spatial and frequency resolution

Spatial resolution is predominantly governed by the focusing power of the dual fiber probe device, resulting in an estimated spatial

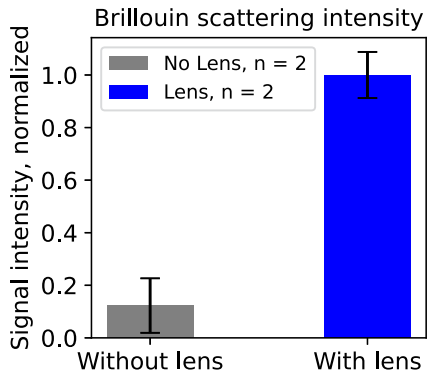

FIG. 8. Signal enhancement by conic off-axis freeform lens, compared to a bare fiber arrangement. A dual fiber arrangement without lens (left, corresponds to Fig. 1(c) and dual fiber arrangement with freeform lens [right, corresponds to Fig. 1(d)].

resolution of our system to be below 10 μm in the lateral direction and 43 μm in the axial direction.

To test the spatial resolution, we performed axial and lateral scans of a chirped patterned polymer sample 3D printed on a glass substrate (Fig. 6). To illustrate the topography of the sample, we performed a measurement with a white light interferometer [Fig. 6(a)]. We acquired a profile of the sample in the Brillouin frequency domain by line-scanning with our probe in the x-direction [Fig. 6(b)]. The 40, 20, and 10 μm wide polymer lines are well resolved in a lateral scan. We observed frequency peaks in the profile at ~5.6 GHz (water) and ~11.3 GHz (IP-DIP polymer). Note that this is the same frequency as would be expected from measurements acquired using a bulk optical system (Fig. 5).

To estimate the probe's axial resolution, we acquired a depth-scan by approaching the glass substrate with our probe in a stepwise fashion, recording the intensity of the water Brillouin peak [Fig. 6(b) red curve] while the probe's focus is moving across the water–glass interface. By taking the derivative of the intensity [Fig. 6(c), blue dashed curve], we calculated the axial resolution of the dual fiber probe to be 43 μm, equal to the FWHM of the negative part of the dy/dx curve in Fig. 6(c).

Acquisition of a 2D image

The Brillouin signal was successfully mapped across several 2D samples in a pointwise scan. Figure 7(a) illustrates a mm scale stereolithography fabricated sample with the letters "UTS." The pixelation/resolution of the Brillouin signal map is limited by the scan step of 0.15 mm.

Figures 7(b)–7(d) illustrate the 2D mapping of water immersed phase-separated DEAD-Box Helicase 4 (DDX4) protein droplets, ranging in scale from about 5–10 μm. The relatively coarse spatial resolution of the probe and high noise levels result in a Brillouin map in Fig. 7(b), making it challenging to distinguish the protein droplets from the surrounding water. Noise-reduction post-processing filtering (more details in the Material and Method section) reveals the presence of protein droplets as indicated in Fig. 7(c). For reference, Fig. 7(e) is a bright field image of the protein droplet sample, providing a visual correlation between the Brillouin map and the physical structure of the sample.

DISCUSSION AND CONCLUSION

In this work, we demonstrate our advancement in fiber-integrated Brillouin imaging. The designed TPL micro-lens is specifically tailored for a dual fiber off-axis approach. By eliminating the parasitic fiber-based background signal and using overlapping focal spots for the emission and collection light paths, our approach resulted in an eight-fold increase in the collection efficiency of the Brillouin scattering signal compared to a reference dual fiber setup without a lens. We achieve resolutions below 10 μm in the lateral and 43 μm in the axial directions in simulations as well as in PSF and Brillouin measurements. Our miniaturized probe has a diameter of 285 μm, which enables new applications in *in situ* biomedical and novel material characterization methods.

Our Brillouin fiber probe design uses standard single-mode, step-index fibers, which are cheap and can be easily combined with standard fiber-optic components such as fiber circulators and couplers, leading to straightforward integration with a Brillouin imaging system. Our use of standard fibers allowed the use of off-the-shelf components to couple the probe to the laser and the spectrometer. This is in contrast to probes using more exotic, hollow-core fibers, which present significant complexities in coupling signals from the hollow core to standard optical components.[10] Our approach allows for a robust measurement system, which may simplify the translation of Brillouin fiber probe applications.

Current limitations of the probe include (1) the absolute signal strength, which is below state-of-the-art bulk-optical Brillouin imaging systems, resulting in long acquisition times, and (2) spatial resolution, which is comparable to other fiber-based endoscopy systems but significantly lower than that in conventional bulk Brillouin microscopy. These issues may be addressed in the future developments through more tailored optical designs. By increasing the NA of the freeform micro-lens, we anticipate an increase in signal intensity and an improvement in spatial resolution. As this design will reduce the depth of focus, it has not been explored in the current study. The proposed design relies on a single optical surface to focus the beam. Other designs are possible, including the use of a stack of multiple optical surfaces shielded to the immersion medium, which may yield an optical design with a significantly higher NA.[16,25]

SUPPLEMENTARY MATERIAL

The supplementary material of this paper provides details on the shape deviation of the Brillouin fiber probe micro-lens. Furthermore, the ray optical design parameters are provided.

ACKNOWLEDGMENTS

The authors have been supported by the Australian Research Council Center of Excellence in Quantum Biotechnology (Grant No. CE230100021), the National Health and Medical Research Council (NHMRC) Development grant (Grant No. 2022337), Ideas (Grant No. 2001646), and Investigator (Grant No. 2008462), the Heart Foundation Future Leader Fellowship (Grant No. 105608), the Hospital Research Foundation project (Grant No. 2022-CP-IDMH-014-83100), Australia-Germany Joint Research Co-operation Scheme (UA-DAAD), Graduate School of Excellence advanced Manufacturing Engineering (GSaME), Grant No. DFG UP31/1 (Terra Incognita, Global Glimpse), BMBF (DAAD PPP Australia 2024, Grant No. 57701620), Baden-Württemberg Stiftung (Elite Program for Postdocs).

AUTHOR DECLARATIONS

Conflict of Interest

Robert McLaughlin is a co-founder and Director of Miniprobes Pty Ltd., a company that develops optical imaging systems. Miniprobes Pty Ltd. did not contribute to or participate in this study. The remaining authors declare no competing interests.

Author Contributions

Joshua Trapp: Data curation (equal); Formal analysis (equal); Investigation (equal); Methodology (equal); Project administration (equal); Visualization (equal); Writing – original draft (equal);

Writing – review & editing (equal). **Hadi Mahmodi**: Data curation (equal); Formal analysis (equal); Investigation (equal); Methodology (equal); Validation (equal); Visualization (equal); Writing – review & editing (equal). **Marco Wende**: Software (equal); Visualization (equal); Writing – review & editing (equal). **Luke McAlary**: Conceptualization (supporting); Methodology (supporting); Writing – review & editing (equal). **Lezanne Ooi**: Conceptualization (supporting); Writing – review & editing (equal). **Jiawen Li**: Conceptualization (equal); Writing – review & editing (equal). **Robert A. McLaughlin**: Conceptualization (equal); Writing – review & editing (equal). **Alois Herkommer**: Conceptualization (equal); Funding acquisition (equal); Project administration (equal); Supervision (equal); Writing – review & editing (equal). **Andrea Toulouse**: Conceptualization (equal); Funding acquisition (equal); Investigation (equal); Methodology (equal); Project administration (equal); Supervision (equal); Writing – review & editing (equal). **Irina Kabakova**: Conceptualization (equal); Data curation (equal); Formal analysis (equal); Funding acquisition (equal); Methodology (equal); Project administration (equal); Resources (equal); Software (equal); Supervision (equal); Validation (equal); Writing – review & editing (equal).

DATA AVAILABILITY

The data that support the findings of this study are available within the article.

REFERENCES

[1] G. Scarcelli and S. H. Yun, "Confocal Brillouin microscopy for three-dimensional mechanical imaging," Nat. Photonics **2**, 39–43 (2008).

[2] K. J. Koski and J. L. Yarger, "Brillouin imaging," Appl. Phys. Lett. **87**, 061903 (2005).

[3] W. H. Goldmann and R. M. Ezzell, "Viscoelasticity in wild-type and vinculin-deficient (5.51) mouse F9 embryonic carcinoma cells examined by atomic force microscopy and rheology," Exp. Cell Res. **226**, 234–237 (1996).

[4] C. Hahn and M. A. Schwartz, "Mechanotransduction in vascular physiology and atherogenesis," Nat. Rev. Mol. Cell Biol. **10**, 53–62 (2009).

[5] E. C. Filipe *et al.*, "Tumor biomechanics alters metastatic dissemination of triple negative breast cancer via rewiring fatty acid metabolism," Adv. Sci. **11**, 2307963 (2024).

[6] P.-J. Wu *et al.*, "Detection of proteoglycan loss from articular cartilage using Brillouin microscopy, with applications to osteoarthritis," Biomed. Opt. Express **10**, 2457 (2019).

[7] G. Antonacci *et al.*, "Quantification of plaque stiffness by Brillouin microscopy in experimental thin cap fibroatheroma," J. R. Soc. Interface **12**, 20150843 (2015).

[8] I. Rudan and K. Y. Chan, "Global health metrics needs collaboration and competition," Lancet **385**, 92–94 (2015).

[9] I. W. Fong, "Emerging relations between infectious diseases and coronary disease and atherosclerosis," CMAJ. **163**(1), 49–56 (2000).

[10] I. V. Kabakova, Y. Xiang, C. Paterson, and P. Török, "Fiber-integrated Brillouin microspectroscopy: Towards brillouin endoscopy," J. Innovative Opt. Health Sci. **10**, 1742002 (2017).

[11] Y. Xiang *et al.*, "Background-free fibre optic Brillouin probe for remote mapping of micromechanics," Biomed. Opt. Express **11**, 6687 (2020).

[12] S. La Cavera *et al.*, "Label-free Brillouin endo-microscopy for the quantitative 3D imaging of sub-micrometre biology," Commun. Biol. **7**, 451 (2024).

[13] J. Li *et al.*, "Ultrathin monolithic 3D printed optical coherence tomography endoscopy for preclinical and clinical use," Light: Sci Appl **9**, 124 (2020).

[14] S. Lightman, G. Hurvitz, R. Gvishi, and A. Arie, "Tailoring lens functionality by 3D laser printing," Appl. Opt. **56**, 9038 (2017).

[15] T. Gissibl, S. Thiele, A. Herkommer, and H. Giessen, "Sub-micrometre accurate free-form optics by three-dimensional printing on single-mode fibres," Nat. Commun. **7**, 11763 (2016).

[16] T. Gissibl, S. Thiele, A. Herkommer, and H. Giessen, "Two-photon direct laser writing of ultracompact multi-lens objectives," Nat. Photonics **10**, 554–560 (2016).

[17] T. J. Nott *et al.*, "Phase transition of a disordered nuage protein generates environmentally responsive membraneless organelles," Mol. Cell **57**, 936–947 (2015).

[18] J. Drozella, A. Toulouse, S. Thiele, and A. M. Herkommer, "Fast and comfortable GPU-accelerated wave-optical simulation for imaging properties and design of highly aspheric 3D-printed freeform microlens systems," SPIE Proc. **6**, 1110506 (2019).

[19] M. Wende, J. Drozella, A. Toulouse, and A. M. Herkommer, "Fast vector wave optical simulation methods for application on 3D-printed microoptics," J. Opt. Microsyst. **4**, 024501 (2024).

[20] M. Schmid, D. Ludescher, and H. Giessen, "Optical properties of photoresists for femtosecond 3D printing: Refractive index, extinction, luminescence-dose dependence, aging, heat treatment and comparison between 1-photon and 2-photon exposure," Opt. Mater. Express **9**, 4564 (2019).

[21] M. Wende, K. Doth, M. Heymann, and A. Toulouse, "3D-printed immersion micro optics," Light Adv. Manuf. **6**, 19 (2024).

[22] G. M. Hale and M. R. Querry, "Optical constants of water in the 200-nm to 200-μm wavelength region," Appl. Opt. **12**, 555 (1973).

[23] H. Gross, W. Singer, and M. Totzeck, *Handbook of Optical Systems, Volume 2: Physical Image Formation* (John Wiley & Sons, Inc., 2006), Vol. 2.

[24] T. Gissibl, S. Wagner, J. Sykora, M. Schmid, and H. Giessen, "Refractive index measurements of photo-resists for three-dimensional direct laser writing," Opt. Mater. Express **7**, 2293 (2017).

[25] J. Li *et al.*, "Two-photon polymerisation 3D printed freeform micro-optics for optical coherence tomography fibre probes," Sci. Rep. **8**, 14789 (2018).

[26] J. R. Sandercock, "Simple stabilization scheme for maintenance of mirror alignment in a scanning February–Perot interferometer," J. Phys. E: Sci. Instrum. **9**, 566–569 (1976).

[27] H. Mahmodi, A. Piloni, R. H. Utama, and I. Kabakova, "Mechanical mapping of bioprinted hydrogel models by Brillouin microscopy," Bioprinting **23**, e00151 (2021).

[28] M. A. Rad *et al.*, "Micromechanical characterisation of 3D bioprinted neural cell models using Brillouin microspectroscopy," Bioprinting **25**, e00179 (2022).